In Situ Chemical Reaction of Nb$_{12}$O$_{29}$ in a High Resolution Gas Reaction Cell Microscope

M. J. Sayagués[1,2] and J. L. Hutchison

Department of Materials, University of Oxford, Parks Road, Oxford OX1-3PH, United Kingdom

Solid-state oxidation–reduction of a nonstoichiometric Nb$_{12}$O$_{29}$ (NbO$_{2.417}$) with monoclinic cell was studied using a JEOL 4000 EX HRTEM equipped with a gas reaction cell in which the oxide was oxidized and then reduced by sequentially introducing O$_2$ and H$_2$. The oxidation yielded other block structures with higher oxygen content. The first step of the oxidation mechanism, involving formation of *lamellar* defects of composition Nb$_{11}$O$_{27}$ (NbO$_{2.450}$), could be elucidated with great certainty. Nb$_{10}$O$_{25}$ (a metastable polymorph of NbO$_{2.500}$) was formed as a final stage of the oxidation process. Subsequent reduction led to a nearly ordered Nb$_{12}$O$_{29}$ phase suggesting that such an oxidation-reduction reaction is a reversible process. When Nb$_{12}$O$_{29}$ was directly reduced, NbO was found to grow on the surface of the crystal. © 1996 Academic Press, Inc.

INTRODUCTION

Only a few years ago, it was impossible to record structural changes at the unit cell level directly while a reaction was being carried out in an electron microscope, but now with the development of a high performance gas reaction cell (GRC) transmission electron microscope (1) such kinds of experiments are viable.

Nonstoichiometry in the Nb–O system has been widely studied, especially with regard to the structural aspects (2–5). The structure of the compounds belonging to this system are known as "block structures" (based upon the ReO$_3$ lattice). The formulae of block structures may be represented in terms of blocks of corner-sharing octahedra $(m \times n)_p$ that they contain, where p = the number of blocks joined together (usually 1, 2, or ∞). If p is finite, tetrahedral sites are created at the free corners. The overall composition of this block type is given by $M_{mnp+1}O_{3mnp-p(m+n)+4}$ and when $p \rightarrow \infty$ becomes $M_{mn}O_{3mn-(m+n)}$. There are a sufficient number of parameters (m, n, and p) involved so that the same chemical formula may be given by different block structures, which may therefore be regarded as polymorphs.

Nb$_{12}$O$_{29}$ belongs to these so-called block structures, and can be described (6) as formed by crystallographic shear (*CS*) in two dimensions, in the ReO$_3$ type, thereby dividing it into columns or blocks of infinite length and of cross section 3 × 4 (NbO$_6$) octahedra. At the shear planes there is a displacement of half an octahedron diagonal along the column axes; thus, the ReO$_3$ oxygen sublattice is left unaltered, but the metal atoms are now at two different
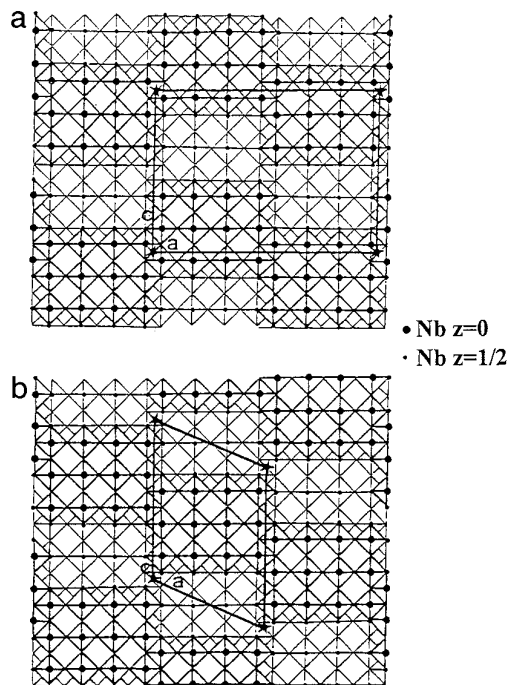

FIG. 1. Idealized structures of (a) orthorhombic (a = 28.90, b = 3.835, and c = 20.72 Å) and (b) monoclinic (a = 15.66, b = 3.832, c = 20.72 Å, and β = 112.93°) Nb$_{12}$O$_{29}$, respectively. The lighter and darker squares represent octahedra of NbO$_6$ which form 3 × 4 blocks by their corner sharing. They are centered about the two levels perpendicular to the *b*-axis and are 1.9 Å apart (4). The unit cells in projection are outlined.
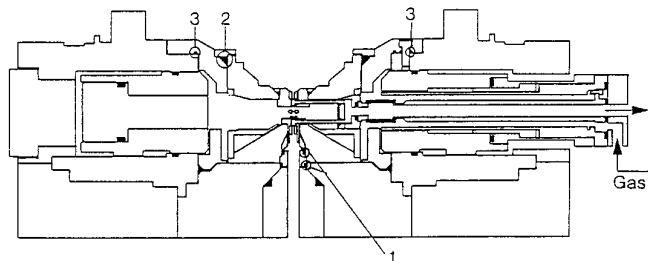
• Nb z=0
· Nb z=1/2

116

FIG. 2. Cross sectional drawing of the electron microscope objective lens area with the cell in position, showing the gas inlet and differential pumping lines connected to the polepiece. 1, 2, and 3 are additional vacuum seals (1).
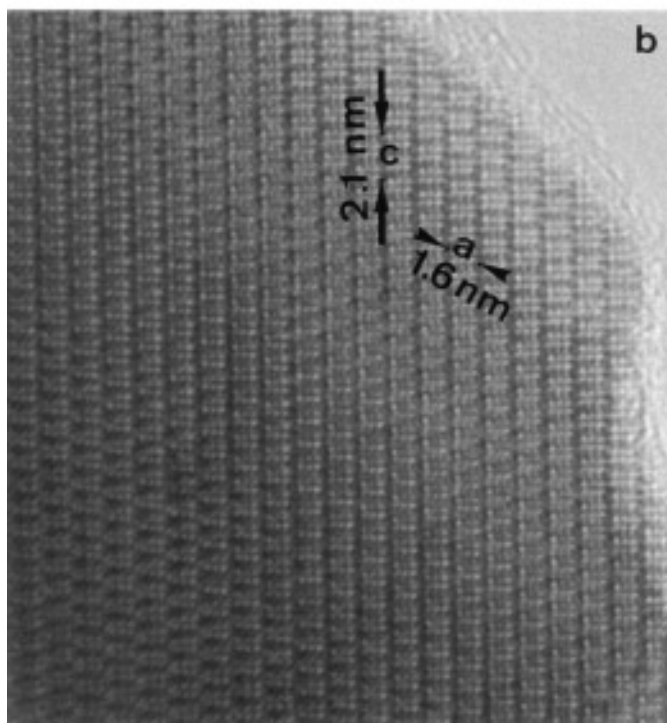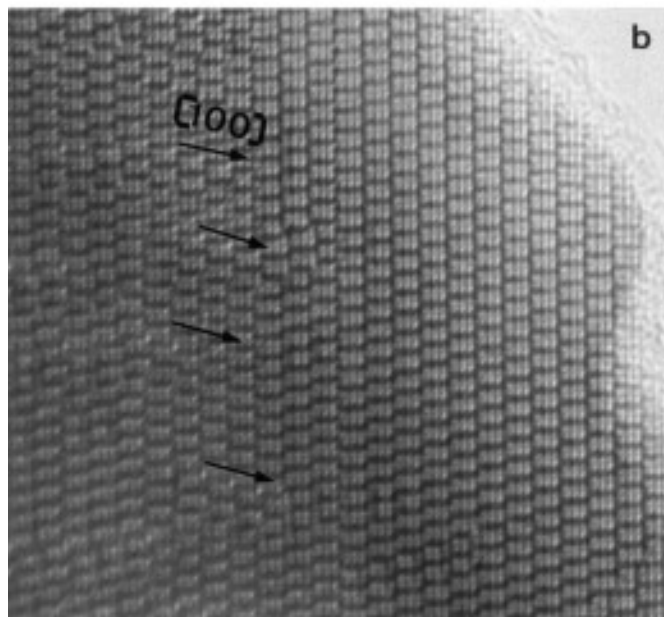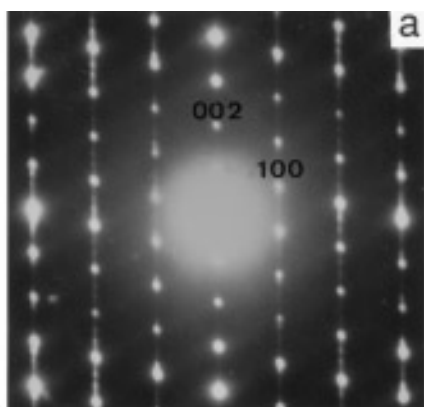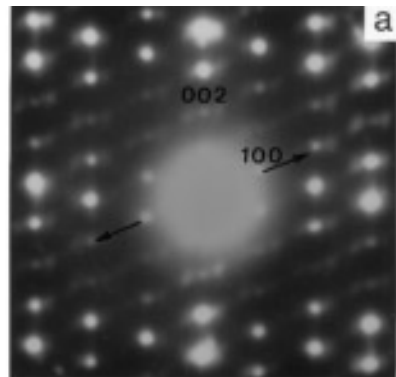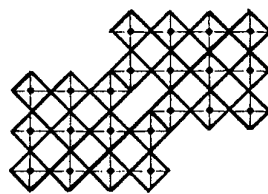

FIG. 3. (a) SAED pattern along $[010]_m$ of a Nb$_{12}$O$_{29}$ crystal under vacuum and (b) corresponding micrograph.

Component of a *lamella* defect
Nb$_{11}$O$_{27}$(NbO$_{2.45}$)

FIG. 4. (a) SAED pattern from the above crystal (same area) after oxidation. (b) Corresponding micrograph; a *lamella* defect (NbO$_{2.45}$) is arrowed along the $[100]_m$ direction. (c) Schematic representation of component of a *lamella* defect.

levels. Wadsley (7) described the dimorphic forms of Ti$_2$Nb$_{10}$O$_{29}$ (orthorhombic: *Amma* and monoclinic: $A2/m$), these being isomorphic with Nb$_{12}$O$_{29}$ (Fig. 1).

The block structures are among the most suitable for detecting subtle changes as a reaction proceeds since they are ideally suited to study by HREM. However, it is difficult (if not impossible) to be sure one is approaching equilibrium in these systems. In 1973 Browne *et al.* (3) studied
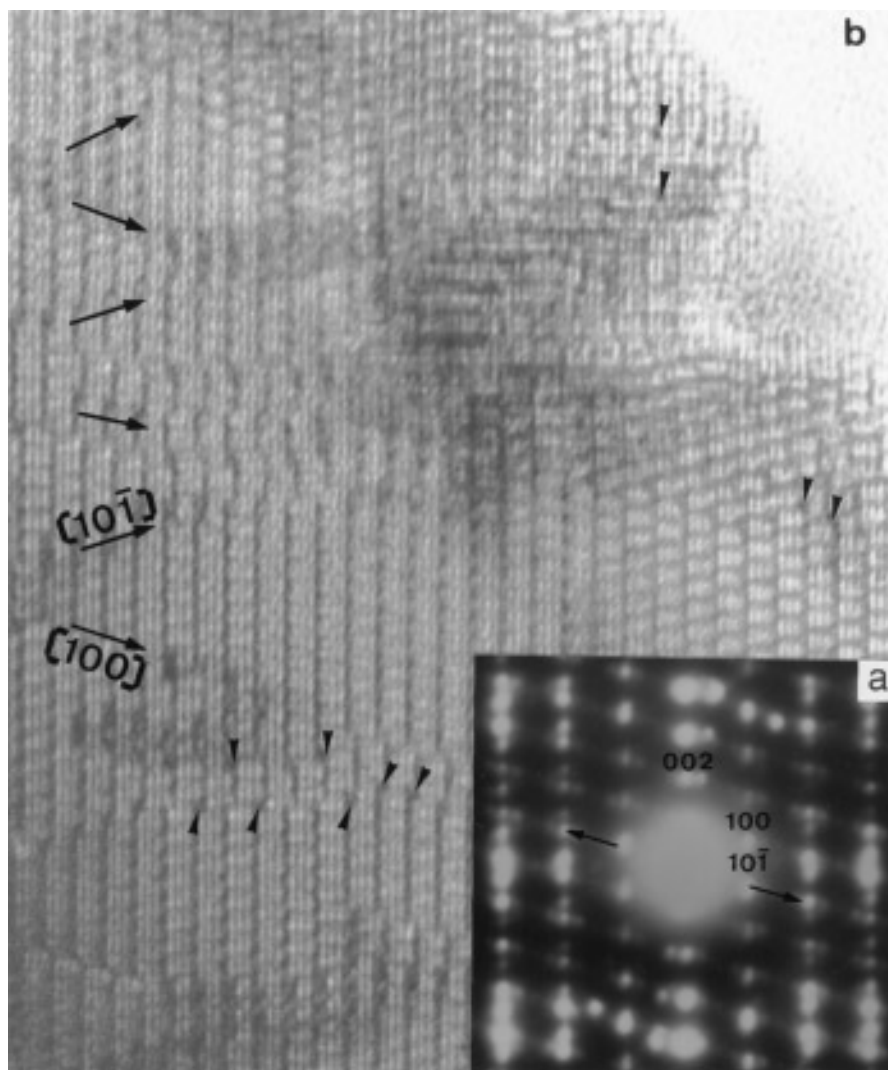
FIG. 5. (a) SAED pattern and (b) corresponding micrograph (same area) after further oxidation. Black contrasts in V shape along $[100]_m$ and $[101]_m$ are marked with large arrows and Nb^{5+} in tetrahedral sites corresponding to $Nb_{10}O_{25}(NbO_{2.5})$ with small arrows.

the solid state oxidation of $Nb_{12}O_{29}$ (monoclinic and orthorhombic) to Nb_2O_5. However, the oxidation process was carried out outside the microscope. In this paper, a microstructural study has been performed on the nonstoichiometric monoclinic $Nb_{12}O_{29}$ ($NbO_{2.417}$) oxide ($a = 15.66$, $b = 3.832$, $c = 20.72$ Å and $b = 112.93°$ (4)), which was oxidized (with O_2) and subsequently reduced (with H_2) *inside* the microscope (using the GRC), in order to compare the images before and after reaction and to obtain information about the mechanisms of change from one phase to another.

EXPERIMENTAL

Samples for HREM were prepared by dispersing a suspension of the powder in acetone onto a holey carbon film

supported by a copper grid. Observations were made using a gas reaction cell microscope based on a JEOL 4000EX (side-entry configuration). The GRC is installed completely inside a standard SAP40 polepiece, which is vacuum-sealed into the objective lens (1). The differentially pumped apertures are sealed vacuum-tight into the upper and lower polepiece bores and pumping line mounted in the polepiece spacer ring (Fig. 2). An important feature of these attachments is that they are all mounted *within* the polepiece, thus facilitating easy insertion of the entire cell into the microscope column, or removal from it, through standard ports. The vacuum connection, which is coaxial with the gas inlet, has a metal bellows to assist alignment and minimize strain, and is screwed into position through a side port.

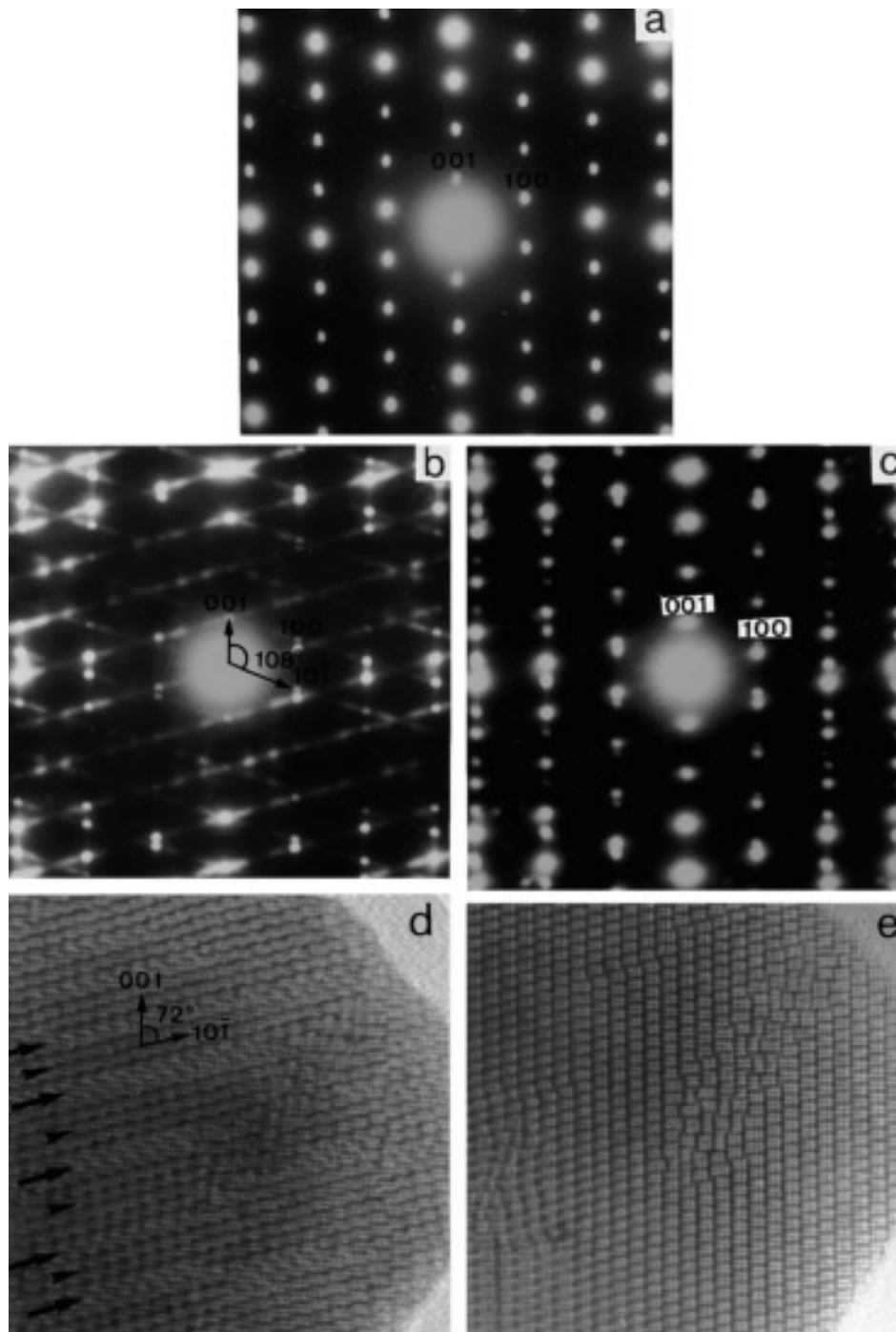The reaction gas was introduced into the chamber and

FIG. 6. Sequence of SAED patterns (a–c) and HREM micrographs (d, e) of $Nb_{12}O_{29}$ crystal along the [010] zone axis. (a) In vacuum. (b) After oxidation (O_2), (d) corresponding micrograph. (c) Further reduction (H_2), (e) corresponding micrograph.

the electron beam was used (by changing the condenser aperture) to heat the crystal. Typical operating conditions included magnifications of 3 to 6×10^5 X with electron current densities for viewing on the TV monitor of 40–60 pA/cm^2, with 15–20 pA/cm^2 for photographic recording.

RESULTS AND DISCUSSION

First Experiment: Oxidation in Several Steps

Figure 3a shows the selected area electron diffraction (SAED) pattern along the $[010]_m$ (subindex ''m'' refers
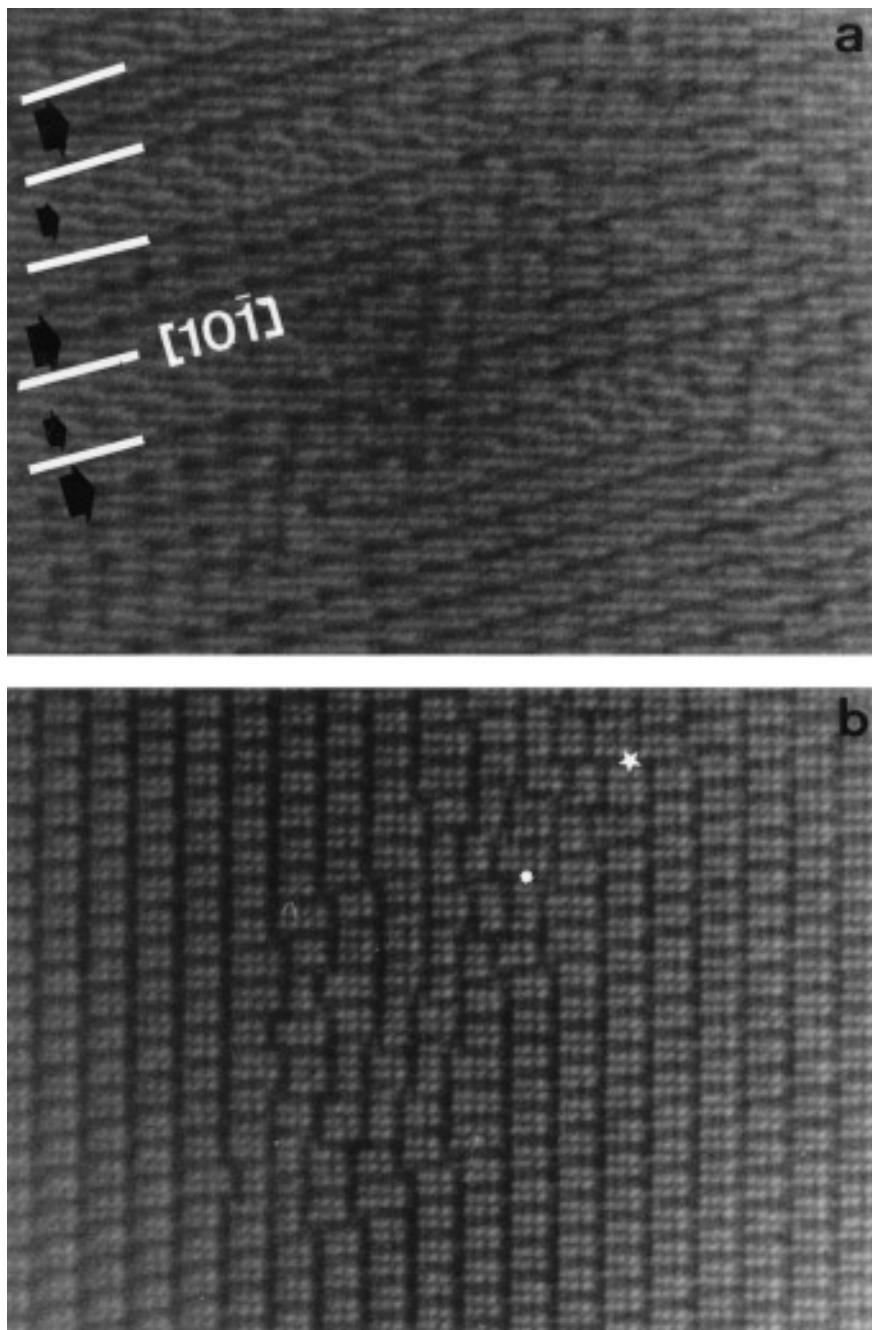
FIG. 7. Enlargements of the micrographs shown in the above figure. (a) After oxidation, $Nb_{12}O_{29}$ structure (small arrows) and $NB_{10}O_{25}$ structure (big arrows) are alternating in fringes along the $[101]_m$ direction. (b) Further reduction; 3×5 (*) and 4×4 (⋆) blocks are marked.

to the $Nb_{12}O_{29}$ structure with monoclinic cell) zone axis from a crystal under vacuum. The corresponding high resolution micrograph is shown in Fig. 3b. The array of cations from the $Nb_{12}O_{29}$ monoclinic structure forming the characteristic 4×3 blocks can be deduced from the 2×3 white dots, which are the channels in each 4×3 block.

The same area was imaged after 10 min of being heated by the electron beam under 15 mbar of O_2. The SAED pattern has changed (Fig. 4a), and very clear streaking in the $[100]_m^*$ direction can be seen. This fact agrees with the appearance in the corresponding micrograph (Fig. 4b) of elongated white contrast linking pairs of 3×4 blocks in the $[100]_m$ direction. This linkage of two 3×4 blocks produces rectangular tunnels as is schematically represented in Fig. 4c. Where several such compound blocks
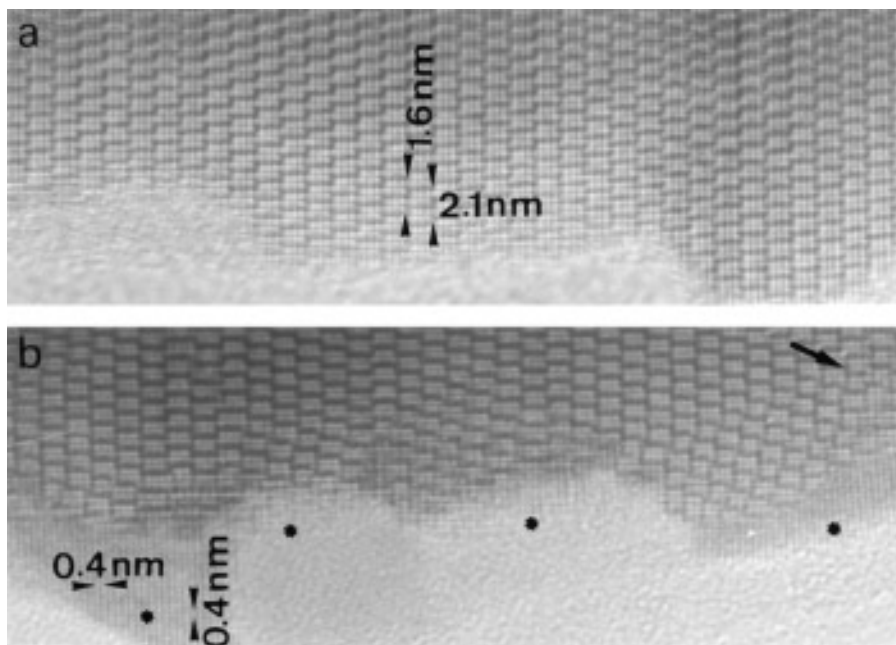
FIG. 8. Micrographs of a Nb$_{12}$O$_{29}$ crystal along [010]$_m$ (a) in vacuum, (b) after reduction (H$_2$), NbO layer can be seen at the surface (*) and some *lamella* defects are arrowed.

are in an ordered aray this is termed a *lamella* defect due to its formation by a cooperative movement of atoms. The nominal composition is Nb$_{11}$O$_{27}$ (NbO$_{2.45}$).

Remarkably, the oxidation reaction appears to be initiated in the bulk, not at the surface as would perhaps have been expected. The formation of *lamella* defects thus seems to be the first stage in the oxidation process and the rectangular tunnels should provide the diffusion paths for the next oxidation stages.

Further beam heating and oxidation led to the SAED pattern and high resolution image shown in the Figs. 5a and b respectively. A change in the streaking direction can be seen in the electron diffraction pattern (Fig. 5a); now it appears along [101]$_m$*. An extended defect in a 'V' array along the [100]$_m$ and [101]$_m$ directions (arrowed) can be observed in the corresponding micrograph (Fig. 5b). The structure involving the *lamella* defects appears to develop local domains of Nb$_{10}$O$_{25}$ structure (a metastable phase of NbO$_{2.5}$), formed by 3 × 3 blocks with some Nb^{5+} in tetrahedral sites, which corresponds to the black spot marked with small arrows in the image. The problem after the second oxidation was contamination; the crystal appears to be covered with an amorphous film, which makes it difficult to distinguish the final structure.

Second Experiment: Oxidation Followed by Reduction

Figures 6a–6c show a sequence of SAED patterns along the [010]$_m$ zone axis for the same crystal and same area obtained in vacuum, after oxidation, and after reduction respectively. The electron diffraction pattern in vacuum (Fig. 6a) corresponds to a characteristic monoclinic Nb$_{12}$O$_{29}$ structure. After 10 min under 15 mbar of oxygen and heating of the crystal with the beam, the electron diffraction pattern shown in Fig. 6b was found. By comparing Figs. 6a and 6b, it is possible to see that a new structure is forming, as can also be appreciated in the corresponding image (Fig. 6d). In this micrograph, an extended defect array is seen, and the structure can be considered to be in the early stages of a superstructure (marked with arrows), where alternating fringes with different contrast can be observed. One set seem to correspond to the Nb$_{12}$O$_{29}$ structure and other to the Nb$_{10}$O$_{25}$ structure. The formation of the Nb$_{10}$O$_{25}$ structure could be the second (or final) stage in the mechanism of the oxidation process. Again, black dot contrast arising from Nb^{5+} in tetrahedral sites (Nb$_{10}$O$_{25}$ structure) can be seen in an enlargement (Fig. 7a) of Fig. 6e.

The crystal was finally reduced under hydrogen (15 mbar for 10 minutes), again using the beam to heat the sample. Figure 6c shows the SAED pattern obtained, which is similar to that found before oxidation, indicating that the crystal has nearly recovered its initial structure. The image in Fig. 6e shows exactly the same area as in Fig. 6d. An enlargement of Fig. 6e is shown in Fig. 7b, where it is easy to notice that the structure is nearly ordered. Only a small area with other kinds of blocks remains: 3 × 5 blocks corresponding to the Nb$_{15}$O$_{37}$ (NbO$_{2.47}$) structure and 4 × 4 blocks corresponding to the Nb$_{16}$O$_{40}$ (NbO$_{2.5}$) structure.

Third Experiment: Aggressive Reduction

A new crystal was observed in vacuum along the $[010]_m$ zone axis (Fig. 8a), showing an ordered image of $Nb_{12}O_{29}$. It was first subjected to slight oxidation, as before. Then after 10 min under H_2 (15 mbar) the structure has started to change *at the surface* (Fig. 8b) (marked by *). This image shows also the local development of 3×3 blocks and *lamella* defects due to the initial oxidation. From the appearance of the surface it is possible to see how the block structure has been destroyed to form an array of octahedra leading to "NbO"—a rocksalt structure (8), which is the most reduced form in the Nb–O system.

CONCLUSIONS

We have observed that the oxidation process (in the first experiment) begins in the middle of the crystal, where it is much thicker (and consequently it is more difficult to observe the changes) rather than at the surface of the crystal. However, in the reduction process (third experiment) the reaction takes place at the surface of the crystal, in fact, NbO (with a simple cubic structure) is formed, rather than another block structure. The oxidation mechanism is a two-step process; the first occurs through the formation of *lamella* defects ($NbO_{2.450}$), a structure with rectangular channels providing the paths for the fast inward diffusion

of oxygen. The second (or final) step leads to the $Nb_{10}O_{25}$ structure, formed by 3×3 blocks and some Nb^{5+} cations in tetrahedral coordination. Both of them are produced along the $[100]_m$ and $[101]_m$ directions. The results of the second experiment suggest that the oxidation–reduction reaction is a reversible process. Further experiments are in progress.

REFERENCES

1. R. C. Doole, G. M. Parkinson, J. L. Hutchison, M. J. Goringe, and P. J. F. Harris, *JEOL NEWS* **30E,** 30 (1992); R. C. Doole, G. M. Parkinson, and J. M. Stead, *in* "Inst. Phys. Conf. Series, No. 118, p. 157. Institute of Physics, Bristol, 1991.
2. R. S. Roth, A. D. Wadsley, and J. S. Anderson, *Acta Crystallogr.* **18,** 643 (1965).
3. J. M. Browne, J. L. Hutchison, and J. S. Anderson, *in* "Proc. 7th Symp. on Reactivity of Solids," p. 116. 1972.
4. S. Iijima, S. Kimura, and M. Goto, *Acta Crystallogr. Sect. A* **29,** 632 (1973).
5. J. S. Anderson, *Chem. Scripta* **14,** 129 (1979).
6. D. M. Adams, "Inorganic Solids: An Introduction to Concepts in Solid-Sate Structural Chemistry." Wiley, Chichester, 1974.
7. A. D. Wadsley, *Acta Crystallogr.* **14,** 664 (1961).
8. M. R. MacCartney and D. J. Smith, *Surf. Sci.* **221,** 214 (1989).